Shift of K x-ray lines associated with valency change and with isomorphous phase transitions in rare earths

O. I. Sumbaev

B. P. Konstantinov Leningrad Institute of Nuclear Physics of the Academy of Sciences of the USSR
Usp. Fiz. Nauk **124**, 281–306 (February 1978)

Studies are reviewed that employ the effect of an anomalously strong shift of the fundamental K-series x-ray lines associated with a change in the number of $4f$ electrons in a given atom for investigating the phenomenon of variable valency in compounds of the rare-earth elements in general, and the so-called isomorphous phase transitions in these compounds in particular. The mechanism of the shift effect and its theory are described. The available data on the shifts of the K-lines of the different compounds of all the rare-earth elements (except promethium) are discussed. A summary table gives the valencies (including the anomalous ones), the occurrence of which has been proved by this method. Application of the K-shift method for studying isomorphous (or isostructural) transitions allows one to establish unambiguously that the mechanism of these transitions involves a change in the number of $4f$ electrons, and to measure the magnitude of these changes. The review concludes with a brief description of the principles and design of the required experimental apparatus-crystal diffraction spectrometers.

PACS numbers: 64.70.Kb, 32.30.Rj, 61.60.+m

CONTENTS

1. INTRODUCTION

The $4f$ shell, which becomes filled in the case of the rare-earth elements, lies deep inside the atom at about the same place as the other, long since filled (s, p, d) shells with the principal quantum number of four. The peak density of $4f$ electrons occurs at a radius several (5–8) times smaller than the radius of the atom determined by the outermost (e.g., 6s) electrons. Hence an electron in a $4f$ state, lacking an opportunity of encountering electrons of neighboring atoms, practically does not participate in forming chemical bonds, i.e., it is not a valence electron. Yet the $4f$ level lies energetically near the levels of the valence $5d$ and $6s$ electrons. These facts are well known, and they arise from the repulsive centrifugal potential, which is proportional to $l(l+1)$, where l is the orbital quantum number, which is three for $4f$ electrons.

The spacing from the $4f$ level to the levels of the valence $5d$ and $6s$ electrons proves to be comparable with the energies released upon forming a chemical bond. Here promotion often proves favorable, i.e., excitation of one of the $4f$ electrons to a valence level. The new (extra) valence bond formed thereby can supply enough energy to compensate for the energy of promotion. Conversely, a change in the parameters of an existing chemical bond (change of partner or even a change in bond length, e.g., upon forced stretching or heating) can make its rupture energetically favorable, with return of the valence electron to the $4f$ level. Therefore, a valency of four or two is observed in a number of cases in addition to the valency of three that is typical of all the rare earths.[1–3] Thus the $4f$ shell plays the role of a sort of "depot." The electrons situated there do not themselves participate in chemical bonding. Yet under the conditions presented above they can shift to the valence band, i.e., become chemically active, or vice versa, they can leave the valence band.

An essential point is that the energy location of the $4f$ level itself proves to depend on the external conditions, primarily on the volume occupied by the atom. It varies by amounts comparable with the energy spacings under discussion even at moderate pressures (units or tens of kilobars). The latter fact, together with the above-noted dependence of the chemical binding energy on the distance between the partners, renders the valency sensitive to such physical factors as pressure and temperature. Bridgman had already observed[4] a phenomenon, which was explained in the early fifties by Pauling and Zachariasen,[5,6] and which has been rather well studied now for metallic Ce[7–9] and SmS.[10–13] It consists of a sharp, discontinuous change in the volume of the specimen, $\Delta V/V \approx 15\%$, at a definite pressure (6–9 kbar). Remarkably, the observed first-order phase transition is not accompanied by a change in structure, i.e., in crystal-lattice symmetry. Hence its primary cause can be only an event on the intraatomic, rather than on the lattice level. Presumably the presented material has already allowed the reader, following the authors of

 0038-5670/78/2102-0141$01.10

Refs. 5, 6, to view these isostructural (or isomorphous) transitions as a special case of the phenomenon of variable valency, which is initiated by physical causes and which consists of a transfer of one of the $4f$ electrons of a rare-earth atom to the valence band. The sharp change in volume is excellently explained quantitatively by the compression of the atoms themselves. After such a transition, the outer electrons of the latter prove to be subject to the action of the increased electric change.

Evidently the valency, i.e., the number m of valence electrons, will be determined in the cases discussed by the relationship

$$m=(Z-Z_{\widetilde{Xe}})-Z_{4f}. \tag{1}$$

Here Z is the atomic number of the element, or the total number of electrons per atom, Z_{Xe} is the number of electrons in the nearest inert core (xenon), and Z_{4f} is the number of electrons in the $4f$ shell. The number in parentheses for a given element is constant. Hence a change Δm in the valency is unambiguously associated with a change ΔZ_{4f} in the number of $4f$ electrons:

$$\Delta m = -\Delta Z_{4f}. \tag{2}$$

The transition of a $4f$ electron to one of the valence levels or the reverse "collapse" of a valence electron into an inner $4f$ state with a severalfold change in the dimensions of its corresponding "orbit" is a unique phenomenon that is catastrophic on an atomic scale. One of its manifestations could be an anomalously strong change in the energy of even the fundamental K_{α_1} and K_{β_1} x-ray lines, which are due to transitions between the innermost levels of the atom ($1s$–$2p$; $1s$–$3p$). Hence these lines are *usually not subject to any influences*. This expectation has been confirmed[14] and has subsequently allowed the effect of shift of the K x-ray lines to be used as a new experimental method of studying the phenomenon of variable valency in the rare-earth elements in general[15–17] and the phenomenon of isomorphous phase transitions in particular.[9,13,18,19]

The present review offered to the readers' attention is a collection of the first results along this line, i.e., an illustration of how the discussed phenomena look, so to speak, *in terms* of the displacements of the x-ray lines.

2. THE EFFECT OF CHEMICAL SHIFT OF K X-RAY LINES

Let us examine (Fig. 1) the potential $U(r)$ due to one of the atomic electrons, e.g., a $4f$ electron, whose radial wave function $\rho(r)\equiv r^2\psi^2(r)$ is shown by the dotted curve. Evidently we have

$$U(r)=\frac{1}{r}\int_0^r \rho(r')\,dr'+\int_r^\infty \frac{\rho(r')\,dr'}{r'} \tag{3}$$

and

$$\frac{dU(r)}{dr}=-\frac{1}{r^2}\int_0^r \rho(r')\,dr'. \tag{4}$$

As we know, the radial wave function of an electron having the principal quantum number n and the orbital quantum number l has $(n-l)$ maxima. That is, it has one maximum for a $4f$ electron. Hence the potential U_{4f} electron. Hence the potential $U_{4f}(r)$ in the region of the inner $1s$, $2p$, and $3p$ shells is constant ($U_{4f}(0)$ in Fig. 1), while the derivative $dU_{4f}(r)/dr$ is zero throughout the region inside the $4f$ shell.

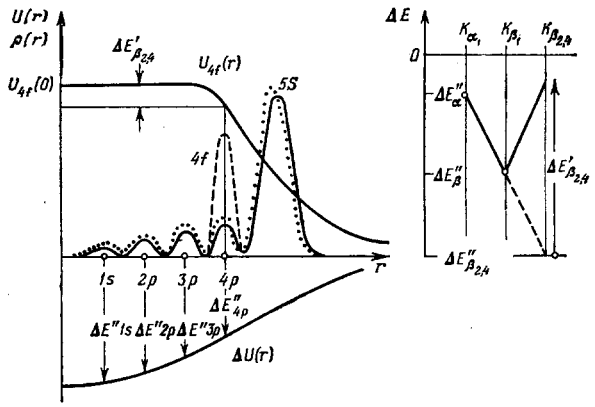

FIG. 1. Explanation of the mechanism of the effect of chemical shift of x-ray lines. $\rho(r)\equiv r^2\Psi^2(r)$—radial density of electrons: $5s$ electron—light solid curve having five $(n-l=5)$ maxima; $4f$ electron—dashed curve having one $(n-l=1)$ maximum; the positions of the principal density maxima for $2p$, $3p$, and $4p$ electrons are also noted; $U_{4f}(r)$ is the potential produced by a $4f$ electron; $\Delta U(r)$ is the change in potential caused by deformation of the wave functions of the electrons upon removing (or exciting) a $4f$ electron (the nature of the deformation for a $5s$ electron is shown by the dotted curve); $\Delta E'_{\beta_{2,4}}$ is the direct change in the energy of the $K_{\beta_{2,4}}$ line upon removing a $4f$ electron; $\Delta E''$ are the changes in energy of the $1s$, $2p$, etc., levels caused by compression of the wave functions of the electrons upon removing a $4f$ electron. The inset at the right shows the relationship between the shift and the line type that is expected upon removing a $4f$ electron.

Removal of a $4f$ electron increases the binding energy of the $1s$, $2p$, and $3p$ electrons by the same amount, which is equal to $U_{4f}(0)$; the spacings between these levels, which define the energies $E_{\alpha_{1,2}}=E_{1s}-E_{2p}$, $E_{\beta_{1,3}}=E_{1s}-E_{3p}$ of the $K_{\alpha_{1,2}}$ and $K_{\beta_{1,3}}$ lines, remain unchanged. Only the $K_{\beta_{2,4}}$ line, which corresponds to a transition from the $4p$ level, undergoes a substantial positive shift: the binding energy of the $4p$ level is increased by a smaller amount than the binding energy of the $1s$ level. Evidently the difference ($\Delta E'_{\beta_{2,4}}$ in Fig. 1) will determine the energy shift of the $K_{\beta_{2,4}}$ line. However, the result of removing a $4f$ electron or transferring it to an outer orbital (e.g., $6s$) is also an increase (almost by unity) in the charge that gives rise to the Coulomb field acting on the outer filled $5s$ and $5p$ shells. The wave functions of the latter, which possess inner maxima, since $n-l=5$ or 4, respectively, are thereby compressed toward the nucleus (see the solid and dotted curves for the $5s$ electrons in Fig. 1). The result will be an introduction into the region of the inner shells of a certain electron charge $\Delta\rho(r)$ and the appearance of a corresponding potential $\Delta U(r)$. Upon looking at Eqs. (3) and (4), we can easily see that this will diminish the binding energy of the inner levels, and the decrease will be maximal for

the innermost, i.e., the 1s level. Correspondingly the energies of the K lines will decrease. That is, the lines will undergo negative shifts that will increase with increasing distance from the nucleus of the outer level of the transition:

$$|\Delta E''_{\beta_{2,4}}|>|\Delta E''_{\beta_{1,3}}|>|\Delta E''_{\alpha_{1,2}}|.$$

The inset of Fig. 1 shows this graphically. However, the monotonic increase of the negative effects will be distorted for the $K_{\beta_{2,4}}$ line by the above-discussed large positive shift $\Delta E_{\beta_{2,4}}$. Hence we can expect upon removing a $4f$ electron a highly characteristic V-shaped pattern of large negative shifts of the K lines, i.e., corresponding to an energy decrease. Conversely, an increase in the number of $4f$ electrons will cause an analogous effect of opposite sign (a positive Λ-shaped shift).

One can predict the shifts of the K lines upon changing the number of $4f$ electrons far more accurately, but less pictorially, by representing the shifts as differences of the corresponding eigenvalues of the energy ε in self-consistent calculations of the Hartree–Fock type:

$$\begin{aligned}\Delta E_{\alpha_{1,2}}&=(\varepsilon_{1s}-\varepsilon_{2p})_{4f^{n-1}}-(\varepsilon_{1s}-\varepsilon_{2p})_{4f^n},\\ \Delta E_{\beta_{1,3}}&=(\varepsilon_{1s}-\varepsilon_{3p})_{4f^{n-1}}-(\varepsilon_{1s}-\varepsilon_{3p})_{4f^n}\ \text{etc.}\end{aligned}\qquad(5)$$

Here the differences in parentheses will represent the energies of the K lines corresponding to configurations having n and $n-1$ $4f$ electrons.[1)] In this way one can expect quite satisfactory predictions, not only qualitatively but also quantitatively. This is because the participants are essentially only the sufficiently internal levels of the atom, and to a very good degree the one-atom approximation is satisfactory for the problem. As we know, the best embodiment of the latter are the Hartree–Fock calculations. Figure 2 presents some results of such calculations,[20] which were specially undertaken for this purpose.[2)] In addition to the already familiar V-shaped relationship that involves removal of one $4f$ electron (the points for Eu^{3+}–Eu^{2+} are connected), the shifts are given that are due to removal of one of the valence electrons, i.e., $5d$, $6s$, or $6p$.[3)] The dotted line and the points with the error bars show the experimental values[14] for EuF_3–EuF_2, which are typical tri- and divalent compounds, and which thus differ in one $4f$ electron.

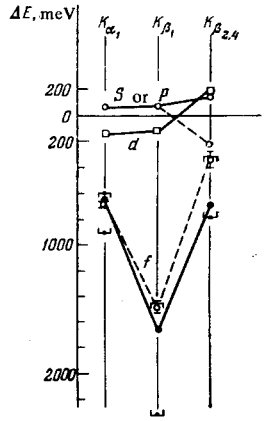

FIG. 2. Typical shift-line type relationships for $4f$, $5d$, and $6s$ (or p) electrons. For the $4f$ electrons, the solid line joins the calculated energy differences of the K lines of europium having the configurations $Eu^{3+}(Xe)4f^6$ and $Eu^{2+}(Xe)4f^7$, while the dotted line joins the experimental shifts for EuF_3 and EuF_2. The brackets indicate the calculated limits of the shifts of the corresponding lines upon removing a $4f$ electron for the other rare-earth atoms (from Ce to Yb).

As expected, one observes good quantitative agreement of the calculated and experimental data. The effects from the $4f$ electrons are anomalously large. They substantially exceed (by a factor of 5–15) the effects due to the valence electrons, and they give a characteristic V-shaped relationship. This completely rules out their simulation by any phenomena of a different nature.

The brackets in Fig. 2 limit the regions containing the calculated shifts[20] for the different rare-earth elements from Ce to Yb. It turns out that the relationships between the shift and the type of line are similar for all the rare-earth elements. Apparently the latter fact should not be surprising, since it stems from the similarity of structure of the inner shells of the atoms, i.e., from the same causes as those responsible for the similarity and simplicity of the x-ray spectra themselves.

3. THE PHENOMENON OF VARIABLE VALENCY OF THE $4f$ ELEMENTS AS REFLECTED IN THE K-SHIFTS

Table I and Figs. 3 and 4 collect the experimental data[17] on the chemical shifts in compounds of the rare-earth elements of different valencies. The reference point from which the shift was measured was in all cases chosen as the simplest trivalent oxides or halides whose valency of three had been firmly established.[4)]

The difference from the reference point in the number of $4f$ electrons, i.e., the difference of the valency from three (see Eqs. (1) and (2)) should give rise to characteristic V-shaped relationships if the valency exceeds three, i.e., approaches four, and to Λ-shaped relationships if the valency is less than three, i.e., approaches two. Comparison of the amplitudes of the curves with the maximum experimental amplitudes, which can be taken as corresponding to a valency change of one, or with the analogous calculated values (see Fig. 2) makes it possible also to estimate directly the fraction of the

[1)] The requirements on the model being used are not very stringent, since the calculations must be carried out accurately by the same program for both configurations being compared. Here the possible errors compensate apart from small errors due to the difference in configurations, i.e., proportional to the sought effect itself. Of course, the numerical accuracy of the self-consistent calculation must be greater than the sought effect, and must amount to a few millielectron-volts.

[2)] The calculations were performed by the Dirac–Slater method, which is a relativistic variant of the Hartree–Fock method with the exchange interaction being taken into account approximately (aPa Thomas–Fermi).

[3)] By employing arguments like those of Fig. 1, the reader can easily understand the characteristic features of these curves also.

[4)] In a number of cases this statement was directly tested within the framework of this same method by measuring the zero shifts that different trivalent compounds should give with respect to one another in this approximation, since it is improbable that a fractional valency differing from three arising from "fortuitous" circumstances would prove to be the same for several tested compounds.

TABLE I. Chemical shifts of K-series x-ray lines in compounds of the rare-earth elements.

Compounds		$\Delta E \equiv E_A - E_B$, meV		
A	B	K_{α_1}	K_{β_1}	$K_{\beta_{2,4}}$
Ce_γ	CeF_3	+29±7	−84±12	
Ce_α	Ce_γ	−173±14	−566±32	−103±73
CeF_4	CeF_3	−602±12	−1727±20	−196±52
CeO_4	CeF_3	−412±9	−1240±25	−288±36
$CeCl_3$ + Ce	CeF_3		+10±17	
$NdCl_3$ + Ce	CeF_3		+26±21	
$Ce(SO_4)\cdot aq$	$CeCl_3\cdot aq$	−439±21	−1322±55	−146±85
Rb_3PrF_7	PrF_3		−1375±36	
PrO_2	PrF_3	−386±5	−1034±9	
$PrCl_2$	Pr_2O_3 («A»)	+30±9	−12±20	−423±22
$PrCl$ (6,6% $NdCl_2$)	Pr_2O_3	+280±9	+734±18	
Pr_{met}	PrF_3	+36±10	−18±18	+260±56
Pr_{met}	Pr_2O_3	+20±15		
Nd_{met}	Nd_2O_3 («A»)	−4±9	−55±25	−22±37
NdS	Nd_2O_3	+62±11	+51±18	
$NdCl_2$	Nd_2O_3	+437±15	+1130±20	+394±68
$Cs_3NdF_{6,5}$	Nd_2O_3		−202±56	
$Rb_3NdF_{6,5}$	Nd_2O_3		−142±59	
Sm_{met}	Sm_2O_3 («B»)	−32±11		
$SmCl_2$	SmF_3	+606±14	+1455±40	+413±54
SmS	SmF_3	+595±20	+1430±38	+556±53
SmS ($p > 9$ kbar)	SmS	−318±43	−926±41	−258±180
SmS (20% CdS)	SmS	−352±15	−923±55	−305±62
Eu_{met}	Eu_2O_3 («C»)	+644±10		
EuF_2	EuF_3	+631±15	+1450±40	+300±65
		+630±100*	+1220±340*	
Gd_{met}	Gd_2O_3 («C»)	−36±12		
$GdCl_2$	GdF_3		+10±27	
GdS	GdF_3		+130±104	
Tb_{met}	Tb_2O_3 («C»)	−19±15		
$BaTbO_3$	$Tb_{oxalate}$	−630±28	−1750±38	−252±76
TbO_2	Tb_2O_3	−452±11	−1207±30	
$TbCl_2$ (33% $DyCl_2$)	Tb_2O_3		+59±45	
$TbCl_2$ (33% $SmCl_2$)	TbF_3		+34±95	
Dy_{met}	Dy_2O_3 («C»)	−10±14		
$DyCl_2$	Dy_2O_3	+435±23	+1146±17	+550±92
DyO_2 (TbO_2)	Dy_2O_3	+29±50		
$Rb_3DyF_{6,5}$	DyF_3		−211±61	
Ho_{met}	Ho_2O_3 («C»)	−1±17		
$HoCl_2$	Ho_2O_3	+317±27	+651±15	+154±100
Er_{met}	Er_2O_3 («C»)	+18±43	−36±39	+213±112
$ErCl_2$	Er_2O_3	+32±34	−15±52	
Tm_{met}	Tm_2O_3 («C»)	−46±16		
TmS	Tm_2O_3	+62±19	+102±40	
TmSe	Tm_2O_3	+114±20	+274±57	+217±82
TmTe	Tm_2O_3	+434±32	+990±55	+602±136
$TmCl_2$	Tm_2O_3	+503±15	+1091±34	+613±110
TmCl (Rb)	Tm_2O_3	+363±40		
Yb_{met}	Yb_2O_3 («C»)	+582±30		
$YbCl_2$	$YbCl_3$	+574±34	+1165±85	
Lu_{met}	Lu_2O_3 («C»)	−3±20		
Lu_{met}	LuF_3	+48±38		

compound with anomalous valency in the specimen or the fraction of a $4f$ electron that has gone into forming a resonance-hybridized valence bond that requires only partial transition of a $4f$ electron to a valence level.[5)] We now comment on these data.

[5)]Unfortunately it does not seem possible to distinguish these two possibilities within the framework of the given method, which determines only the position of the "center of gravity" of a line that is displaced but not resolved into components (see Sec. 5 below).

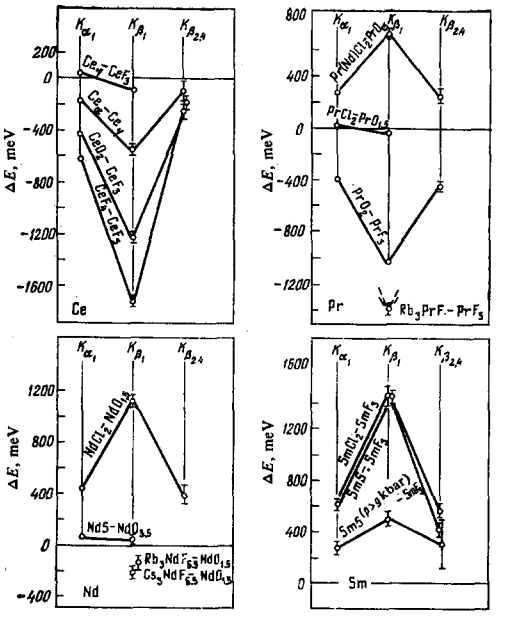

FIG. 3. The phenomenon of variable valency for the elements from Ce to Sm in the shifts of the K x-ray lines. ΔE is the shift of the K line of the element in a compound from its position in a reference trivalent compound. (In the right upper diagram, the lower point refers to Rb_3PrF_7–PrF_3.)

Cerium

The largest shift is seen in CeF_4. Apparently the configuration in this compound is close to $4f^0$, i.e., here a complete transition occurs of the single $4f$ electron into the valence band, and the valency is four. The valency of metallic Ce_γ is close to three, or perhaps, judging from the non-zero negative shift of K_{β_1} (see Table I), which amounts to ≈5% of the shift for CeF_4, it barely exceeds three. We shall return again to metallic Ce_γ and Ce_α in the next section devoted to isomorphous phase transitions; for the present we shall only state that Ce_α

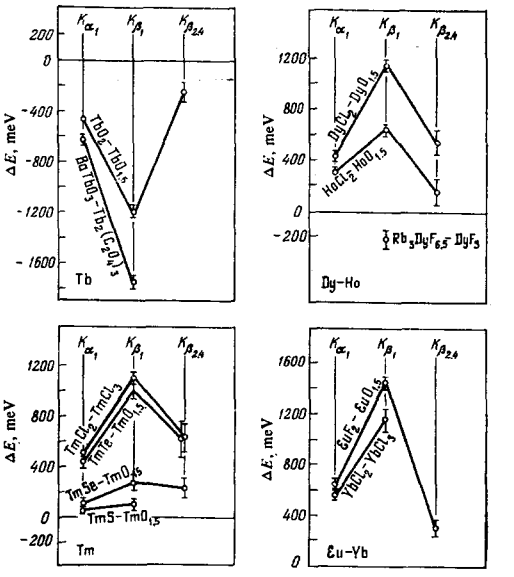

FIG. 4. The same as Fig. 3, but for the elements from Eu to Yb.

shows an appreciable loss of $4f$ electrons as compared with Ce_γ, which amounts to about a third of an electron, and which correspondingly implies a valency close to 3.3.

The appreciable departure from the limiting effect in CeO_2 is highly curious and unexpected.

Praseodymium

Above all, the noteworthy thing here is the simultaneous existence of three valence states, and correspondingly, the only simultaneous observation in our collection (i.e., for a given particular element) of V- and Λ-shaped curves. Metallic praseodymium (see Table I) is trivalent, and it proves to be trivalent also in $PrCl_2$, evidently by forming a bridge compound with a metal–metal bond, which we can provisionally exhibit in the form $Cl_2 = Pr - Pr = Cl_2$. Yet addition to $PrCl_2$ of even a few percent of $NdCl_2$ elicits a quite distinct ($\approx 50\%$) appearance of the divalent form of praseodymium.

Just like CeO_2, PrO_2 does not attain the limiting value of the effect, which is approximated only by Rb_3PrF_7.

Neodymium

Metallic neodymium is trivalent, and neodymium is also trivalent in NdS. However, in contrast to $PrCl_2$, the valency of $NdCl_2$ is close to two.

An attempt to obtain by analogy with Rb_3PrF_7 tetravalent neodymium in $Rb_3NdF_{6.5}$ and $Cs_3NdF_{6.5}$ gave an indefinite result: perhaps a small admixture (at the level of $\approx 10\%$) of the tetravalent state is observed, but the total effect hardly exceeds three standard errors.

Samarium

Metallic samarium is trivalent. Samarium in $SmCl_2$ is divalent, and the same is true of SmS under normal conditions. Yet SmS with a 20% admixture of GdS approaches trivalency. The same effect is produced by application of hydrostatic pressure ($p > 9$ kbar). The nature of these latter phenomena will be discussed in greater detail in the section on isostructural phase transitions.

Europium

Metallic europium, and also EuF_2, are typically divalent compounds.

Gadolinium

Gadolinium is trivalent in the metal and in the compounds $GdCl_2$ and GdS.

Terbium

Metallic terbium is trivalent.

Most interestingly, like CeO_2 and PrO_2, TbO_2 does not attain the limiting shift value. Apparently there is a mechanism of forming a fourth valence bond common to these compounds that is more complex than transition of an entire $4f$ electron to the valence band, and which requires only partial (on the average) $4f \rightarrow 5d$ (or $6s$) transition.

Attempts to obtain the divalent state of terbium in $TbCl_2$ by adding $DyCl_2$ or $SmCl_2$ (see Table I) have failed—Tb remained trivalent.

Dysprosium and holmium

Metallic dysprosium and holmium are trivalent. The existence of valency two is clearly marked in $DyCl_2$ and $HoCl_2$. An attempt to get the tetravalent state of dysprosium in $Rb_3DyF_{6.5}$ gave a result just about as indefinite as in the case of the analogous compounds of neodymium.

Erbium

Metallic erbium is trivalent, and it remains trivalent in $ErCl_2$.

Thulium

Metallic thulium is trivalent.

The valency is close to two in $TmCl_2$.

The behavior of the valency of thulium in the chalcogenides TmS, TmSe, and TmTe is quite remarkable. Here one observes a gradual transition from the practically trivalent state in TmS through a mixed state in TmSe to the practically divalent state in TmTe. Apparently this is an example of the effect of the length of the extra metal–metal bond on its realizability: this distance is least in TmS, and this is probably a typical bridge compound $S = Tm - Tm = S$; in TmSe and especially in TmTe, the possible Tm–Tm distance increases, the extra bond becomes unfavorable, and the electron fully or partially returns to the $4f$ shell to give rise to a marked Λ-shaped relationship.

Ytterbium

Metallic ytterbium is divalent, as is ytterbium in $YbCl_2$.

Lutetium

Metallic lutetium, not strictly being a $4f$ element, is trivalent.

Thus even a qualitative examination of the data on the chemical shifts has allowed us to draw a number of conclusions. Some of them are trivial, while others are perhaps more unexpected. An essential point is that they have all been obtained by a single method within the framework of a completely identical theory. By confirming one another in this manner they provide a unified picture of the valence properties of the rare-earth elements. The most direct result is the unambiguous proof of the realizability in the rare earths of the valencies listed in Table II, which had given rise to some disputes and dissension prior to these studies.[1–3]

4. ISOSTRUCTURAL PHASE TRANSITIONS

The theory of isostructural phase transitions is at present quite well developed. Most of the studies are

TABLE II. Valencies of the rare-earth elements as observed by the method of K x-ray line shifts.

	Ce	Pr	Nd	Sm	Eu	Gd	Tb	Dy	Ho	Er	Tm	Yb	Lu
m	4 3	4 3 2	3 2	3 2	3 2	3	4 3	3 2	3 2	3	3 2	3 2	3

based on examining the system of interacting $4f$–$5d$ (or 6s) electrons, essentially by developing the ideas of Anderson's classical study.[21] They have the aim of explaining with an appropriate choice of parameters the fundamental features of the pressure-temperature phase diagrams of metallic cerium and SmS (see, e.g., Refs. 8, 22).

We shall not present here the contents of this group of studies, since our aims are better served by a somewhat different theoretical approach that was first applied, insofar as we know, to cerium by Waber, Liberman, and Cromer.[23] Here one can obtain simultaneously the energies of the x-ray lines, and a direct experimental test of the theory by the method of x-ray line shifts[24] becomes possible. The latter is important because, apart from certain details of the phenomenon, which can prove convenient for study by virtue of the specifics of the new method, the main point for which the method offers especially convenient proof has remained not fully proven: one still encounters a viewpoint that denies the very $f \to d(s)$ mechanism in the generally accepted sense,[25] and which, in particular, rests on experimental studies in which a $f \to d(s)$ mechanism in the Ce_γ–Ce_α transition was not found.[26–28]

Following Ref. 9, let us examine the results of a Dirac–Slater self-consistent calculation. This calculation is quite analogous to that performed in Refs. 20 and 24, data from which we have employed above (see Fig. 2), but it has different boundary conditions. In earlier calculations people had simulated a free atom, and hence they imposed boundary conditions at infinity.

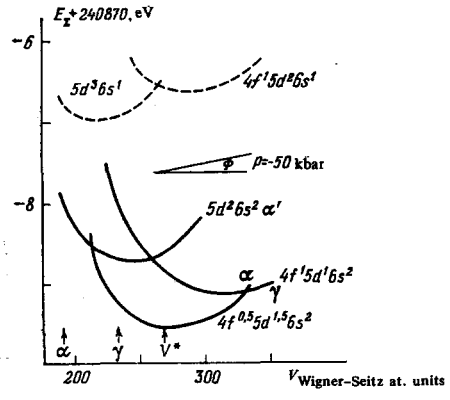

FIG. 5. Total energies E_Σ of cerium atoms in different values configurations as functions of the volumes V of the atoms as calculated by the Dirac-Slater method under the Wigner-Seitz boundary conditions. The scale of the slope angle of the tangent to the curves corresponding to a pressure of 50 kbar is also shown.

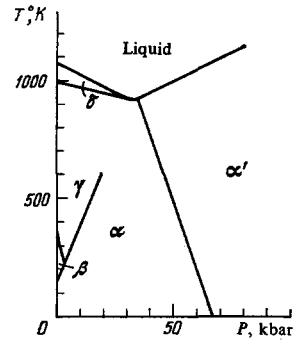

FIG. 6. Phase diagram of metallic cerium. Phases γ, α, and α' are face-centered cubic, the β phase is hexagonal close-packed, and the δ-phase is body-centered cubic.

Now we shall try to describe an atom of the crystal (metal) structure surrounded by like atoms. The volume allotted to a given atom is naturally bounded by planes perpendicular to the line segments linking it with its nearest neighbors and passing through their midpoints. If for simplicity we replace the obtained polyhedron with a sphere of equal volume V with the radius R, and impose boundary conditions on the surface of this sphere so that the sphere should be an impenetrable boundary of the atom, we gain the possibility of accounting for intraatomic properties such as the eigenvalues ε, the total energies E_Σ, the electron density at the nucleus, etc., as functions of V or R. Here we must assign a valence configuration (the number of valence electrons, and hence also that of $4f$ electrons, and their distribution over the valence levels) as a parameter.

The relationship of the total binding energy of the cerium atom thus calculated to the atomic volume V is shown in Fig. 5 for three configurations (solid lines): two integer-valued—trivalent $4f^15d^16s^2$ and tetravalent $4f^05d^26s^2$, and one fractional—$4f^{1-\eta}5d^{1+\eta}6s^2$, where $\eta = 0.5$ and the valency is 3.5. We shall use the trivalent configuration to simulate Ce_γ, the tetravalent configuration to simulate a somewhat hypothetical $Ce_{\alpha'}$,[29] and the fractional configuration to simulate Ce_α. Let us

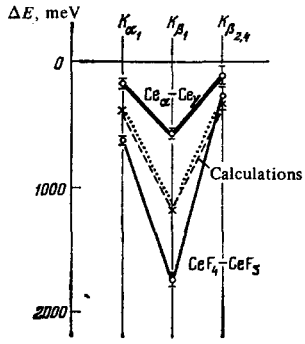

FIG. 7. Calculated and experimental facsimiles (solid lines) for the Ce_γ–Ce_α transition. The solid heavy line joins the experimental shifts of the K lines upon cooling metallic cerium from room temperature to liquid-nitrogen temperature (77°K), the dashed and dotted lines are the calculated shifts under the boundary conditions on the Wigner-Seitz sphere and at infinity, respectively under the assumption that the transformation involves transition of 0.5 $4f$ electrons; the thin solid line gives the experimental energy differences of the corresponding lines for CeF_4 and CeF_3.

find which properties of the phase diagram we can extract from this calculation and compare them with the experimental $p-T$ diagram of cerium (Fig. 6).

First we note that evidently calculations of this type pertain to the case of a fully "frozen" lattice, i.e., they are most closely realized at a temperature of absolute zero. The pressure in the graph of Fig. 5 is defined by

$$P_{T=0} = -\frac{dE_\Sigma}{dV}, \qquad (6)$$

i.e., it is defined as the negative of the slope of the tangents to the $E_\Sigma(V)$ curves. The phase of fractional valency possesses minimal energy at zero pressure (or normal atmospheric pressure, which is the same on the given scale), i.e., the minimum of its total energy occupies the deepest position. Thus, in agreement with experiment (see Fig. 6), the theory predicts that α-cerium is most stable at low temperatures.[6)] One can easily trace in Fig. 5 the qualitatively quite understandable (see above) sharp differences in the radii of atoms having different $4f$ configurations in terms of the shifts in the minima of the total energy toward smaller volumes as the $4f$ electron is removed. We note that the presented theory starts, as one says, from first principles, and contains no parameter other than the mixing parameter η, which in a first crude approximation can be taken to be 0.5.[7)]

Evidently, one can now again use Eq. (5). When one has obtained the energy differences of the K x-ray lines of the studied phases directly within the framework of this calculation, one can compare them with the experimental data and with those calculated earlier in the isolated-atom approximation (with boundary conditions at infinity). Figure 7 makes such a comparison, where the dashed lines join the points pertaining to the energy differences of the K lines calculated at the minima of the Ce_α and Ce_γ curves of Fig. 5. The dotted curve shows the results of a calculation for the same configurations in the free-atom approximation. The solid heavy curve gives the experimental results,[9] which were obtained by comparing the energies of the K_{α_1}, K_{β_1}, and $K_{\beta_{2,4}}$ lines of initially identical specimens of metallic γ-cerium, one of which was kept at room temperature, while the other was cooled to liquid-nitrogen temperature.

First of all we state that both of the calculated facsimiles[8)] of the $4f$ electrons resemble one another in shape and absolute magnitude; evidently here also the fact is manifested that the effect is due to the electrons of the inner shells. Thus it is immaterial in the first approximation which boundary conditions, i.e., which atomic radius, we take for considering the effect of removing a $4f$ electron. Moreover, as we have noted briefly in the last section (see Fig. 3), the $\gamma-\alpha$ transition in Ce undoubtedly involves a decrease in the number of $4f$ electrons. This is eloquently witnessed by the experimental curve of Fig. 7. Thus the studies that deny the fact of transition of an electron from the $4f$ state to the conduction band in cerium[26-28] are in error.[9)] The fraction of this transition expressed as the quantity η (see above) can be refined by using the ratio of the experimental and calculated shifts:

$$\frac{\eta}{0.5} = \frac{\Delta E_{\text{exp}}}{\Delta E_{\text{theor}}}.$$

The weighted mean as found taking into account the experimental errors for the three K lines proves to be

$$\eta_{Ce_\gamma - Ce_\alpha,\ T=77\,^\circ K} = 0.23 \pm 0.02. \qquad (7)$$

The thin solid line in Fig. 7 also gives the experimental relationship for CeF_4-CeF_3 (see Fig. 3). One can employ it to get an estimate of η, which does not depend on the calculations, according to the relationship

$$\eta = \frac{\Delta E_{\text{exp},\ Ce_\gamma - Ce_\alpha}}{\Delta E_{\text{exp},\ CeF_4 - CeF_3}}.$$

Here we find

$$\eta_{Ce_\gamma - Ce_\alpha,\ T=77\,^\circ K} = 0.31 \pm 0.02. \qquad (8)$$

Both values agree rather well, so that we can state that the $Ce_\gamma-Ce_\alpha$ transition at 77°K is accompanied by a transition of from 0.25 to 0.3 $4f$ electron per atom on the average into the conduction band.

Let us proceed to the data involving the phase transition in SmS. Figure 8a shows how this transition looks at room temperature and under pressure "in the light of" the K_{β_1} x-ray line (dark and open points with error bars).[13,18] The dashed line shows the data of Ref. 12, whose authors measured the pressure dependence of the magnetic susceptibility. (The ordinate scales are ad-

---

[6)] Evidently this model does not take into account the extra energy that is released as a result of the extra valency in Ce_α and $Ce_{\alpha'}$, and which depresses the position of the minima for Ce_α and $Ce_{\alpha'}$ (see above, Sec. 1, Introduction).

The pictorial mechanism mentioned in the Introduction of the variation in the position of the $4f$ level with varying pressure (decrease in its binding energy with decreasing atomic volume) can be traced well in studying the relationship $\varepsilon_{4f} = f(V)$ obtained in these calculations (see, e.g., Fig. 5 in Ref. 23). Yet qualitatively the conclusion that the spacing between the $4f$ and $5d$ levels diminishes upon compressing the atom because of the more substantial decrease in the binding energy of the deeper $4f$ electron follows directly from Eqs. (3) and (4) and from a treatment of the type of Fig. 1, where the potential $\Delta U(r)$ is now determined by the charge "squeezed" into the atom as it is compressed.

[7)] Perhaps it is pertinent to note here that in a single center spherically symmetrical problem in the approximation under consideration, the mixing of f and d (or s) levels, that are levels of different parity [$(-1)^3$ and $(-1)^2$ or $(-1)^0$], could stem only from a cause such as neutral weak currents (see, e.g., Ref. 30). Of course, in a polyatomic system such as a real crystal, one need not adduce such an exotic notion, and f-d mixing arises from participation of neighboring atoms.[21]

[8)] This designation[14] is sometimes used for curves of the type of Fig. 2; in the American literature[31] it is translated as "fingerprint." Both terms are rather expressive, and emphasize well the possibility of using these curves for identifying the type of electron that has taken part in forming a chemical bond.

[9)] A possible source of the errors is explained in Ref. 9.

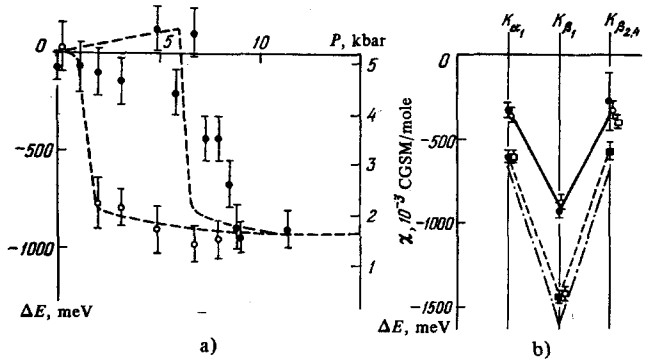

FIG. 8. a) Isomorphous phase transition under pressure in SmS "as seen by" the K_{β_1} x-ray lines (points with error bars—experimental changes ΩE in the energy of the K_{β_1} x-ray line of samarium in SmS upon increasing (solid dots) and decreasing (open dots) the hydrostatic pressure P: the dashed line is inserted for comparison of the data on the magnetic susceptibility χ[12]); b) experimental facsimiles for the isostructural phase transition in SmS (solid circles—transition under hydrostatic pressure, open circles—transition caused by adding gadolinium (20% Gd); the dashed line joins the experimental points for SmF_3–$SmCl_2$ (open squares) and SmF_3–SmS (solid squares); the dot-dash line joins the calculated points for the configurations $4f^5 5d^1$ and $4f^6 Sm^{2+}$).

justed by calculating the best fit of the curves.) The similarity of the x-ray and magnetic curves allows us to judge them to have a common source. Figure 8b (solid curve, solid circles) gives the relationship between the shift and type of line; here one of the initially identical SmS specimens being compared was at atmospheric pressure, and the other at a pressure of about 9 kbar. The dotted line in the same diagram shows the experimental variation for SmF_3–$SmCl_2$ (open squares) or for SmF_3–SmS (solid squares), which are already familiar to us from Fig. 3, together with the relationship calculated for the configurations $4f^5 5d^1$ and $4f^6 Sm^{+2}$ by the Dirac-Slater method.[20] The latter can be used as calibration curves that differ by a single (whole) $4f$ electron. A simple comparison unequivocally indicates the mechanism of the phase transition. The fraction η of the $4f$ transition, which we can easily find from the ratio of the shifts corresponding to the phase transition and to the experimental calibration curve, amounts to

$$\eta_{SmS,\ p\approx 9\ kbar} = 0.62 \pm 0.03 \text{ electron/atom} . \quad (9)$$

If we use the theoretical curve for calibration, we find

$$\eta_{SmS,\ p\approx 9\ kbar} = 0.53 \pm 0.02 \text{ electron/atom} . \quad (10)$$

A method is known for simulating the action of hydrostatic pressure. In simple terms it consists of incorporating the crystal lattice being studied into another one that is somewhat cramped with respect to it, so that crystallization leads to compression. A classical example is the so-called Laves phases (see, e.g., Ref. 32). Another way to bring the atoms of a studied lattice closer together, which also simulates to some extent the action of omnidirectional compression, is to introduce into the lattice replacement atoms of smaller radius than the original ones. The substituents cause a local contraction of the lattice (in particular, see Ref. 33, which directly pertains to the case of SmS of interest to us). At times these methods are very simple and effective. Yet the question always arises of how valid is the model that equates their action to that of simple hydrostatic compression. We find it intriguing to take up some examples that analyze this problem as applied to phase transitions in cerium and SmS by the method of K-line shifts.

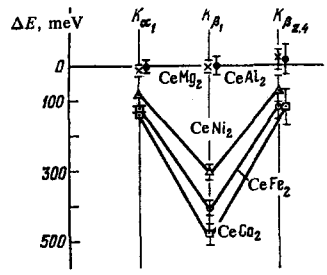

FIG. 9. Facsimile for the Laves phases of cerium. The shifts are measured with respect to Ce_γ.

Figure 9 shows the experimental facsimiles obtained with the Laves phases of cerium.[9] In $CeFe_2$, $CeCo_2$, and $CeNi_2$, the Ce–Ce distance is substantially smaller

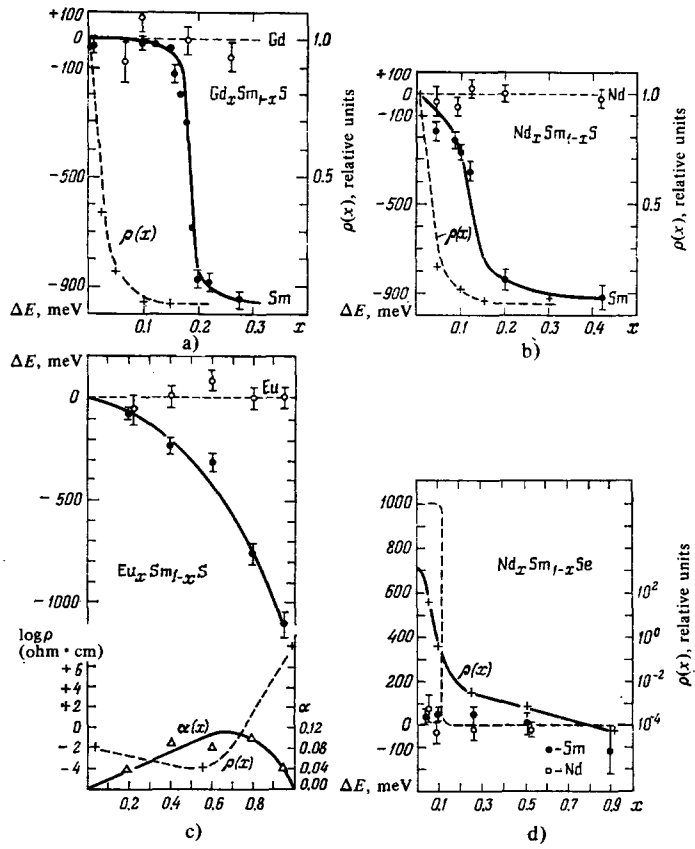

FIG. 10. Relationships of the shifts of the K_{β_1} line of samarium (solid dots with error bars) to the concentration x or the impurity in the compounds (a) $Gd_xSm_{1-x}S$, (b) $Nd_xSm_{1-x}S$, (c) $Eu_xSm_{1-x}S$, (d) $Nd_xSm_{1-x}Se$. The open dots give the shifts of the K_{β_1} lines of the impurity atoms, and the crosses give the resistivities of the specimens; the dashed line in Fig. (d) shows the approximate course of the shift of K_{β_1} of Nd that would have occurred if the semiconductor-metal transition were caused by an electronic transition of neodymium from the divalent to the trivalent state. The triangles in Fig. (c) show the fractions $\alpha(x)$ of trivalent samarium atoms in the total number of rare-earth atoms in the specimens.

than in Ce_γ, i.e., cerium seems to be compressed. Conversely, in $CeAl_2$ and $CeMg_2$ the distances are the same as in Ce_γ or even somewhat larger. Thus one would expect in the former three substances a $4f$ transition analogous to that observed under pressure, while in the latter nothing should happen. We see that experiment has generally confirmed the expectations, but with unexpected details that consist of a certain difference in the effects in $CeFe_2$, $CeCo_2$, and $CeNi_2$. If the latter does not involve defects in the specimens, then it requires a special explanation, since one cannot explain this difference by a simple difference in the effective pressures.

Figure 10 presents a collection of data[19] obtained by the second of the above-mentioned methods of simulating pressure. They pertain to the phase transition in SmS, which was first observed under these conditions in Ref. 33.

In the first case (Fig. 10a), the Sm atoms are partially replaced by Gd, so that we can write the obtained compound in the form $Gd_xSm_{1-x}S$. One measures as a function of x the shift ΔE of the K_{β_1} line of samarium (solid curve, solid points). The shift remains constant in the range $0 \leqslant x \leqslant 0.12$, and undergoes a very sharp jump near $x = 0.18$. Its facsimile is shown by the open circles in Fig. 8b, which excellently fit the curve pertaining to the phase transition under pressure. Thus the phase transitions effected by doping with gadolinium and by applying pressure actually appear similar.

The method offers an opportunity of convincing oneself directly that gadolinium plays the role of a pressure simulator, yet without participating *per se* in the electronic transformations. Upon fixing on the K_{β_1} line of gadolinium and measuring its shift (with respect to a GdS standard) in the transition region (dotted curve, open points), we find practically zero shifts.

If this is actually the role of gadolinium, then we can successfully replace it with another analogous element, e.g., neodymium. The behavior of the $Nd_xSm_{1-x}S$ system (see Fig. 10b) actually proves to be very similar, though not identical. Neodymium also plays a passive role here (Fig. 10b, open points).

The dotted curves in Figs. 10a, b show the resistivities of the studied specimens. These relationships, which are practically identical in both cases, characterize the semiconductor-metal transition that is well known in these compounds. We see that here it bears no relation to the isomorphous transitions (it happens in another range of concentration x) and it can be explained[34] by "short-circuiting" of the semiconductor lattice of SmS by conductive Nd–Nd bonds introduced by the bridge structure S = Nd – Nd = S of trivalent NdS (or GdS).

Figures 10c, d give the results of studies of systems involving substitutions somewhat more radical than those in cases a and b. In the case of Fig. 10c, an attempt to "compress" the SmS lattice was made by adding EuS. In contrast to GdS and NdS, europium is divalent in EuS, but owing to the so-called lanthanide contraction, it has a radius somewhat smaller than Sm.[10] Here also one observes an isomorphous phase transition that reveals itself in the appearance of large negative shifts in K_{β_1} of Sm. However, in this case it occurs smoothly and extends over the entire range $0 \lesssim x \lesssim 1$. As had happened in Gd and Nd, no electronic rearrangement occurs in europium (see the practically zero shifts of the open points in Fig. 10c). A semiconductor-metal transition also occurs here (see the dotted curve for $\log\rho$), but only the trivalent Sm that is formed in the isomorphous transition can short-circuit the lattice. The solid curve with the triangular points in Fig. 10c shows the fraction α of trivalent Sm atoms in the total amount of rare-earth atoms in the lattice. In addition to the value of $1 - x$, the quantities used to calculate it are the fractions η of the trivalent state in the total amount of Sm atoms, i.e., the quantities η (see above) that determine the ratios of the experimental shifts ΔE_{β_1} to the calibration shifts for SmF_3–$SmCl_2$ (see Table I). The minimun resistivity approximately coincides with the maximum of the α curve, while the attained values $\alpha_{max} \approx 0.10$ exactly correspond to the critical concentration of "open valves" needed for electrical short-circuiting of the lattice (see, e.g., Ref. 34).

The case of Fig. 10d is closest to Fig. 10b, but sulfur is replaced by its analog selenium. The experimental shifts of Sm and Nd remain close to zero, i.e., now no isomorphous phase transition occurs. Apparently the Sm–Sm distance is SmSe increases so much as compared with that in SmS that formation of the corresponding bond becomes unfavorable throughout the range of concentrations of the compressing trivalent Nd.[11]

The semiconductor-metal transition ($\rho(x)$ curve) occurs at about the same concentrations as in the case of sulfur (cf. Fig. 10b). Undoubtedly it involves a simple short-circuiting mechanism. The dotted curve shows the approximate course of the K_{β_1} shifts in Nd that would occur if, as was assumed in one of the studies,[35] the semiconductor-metal transition were accompanied by a transition of neodymium from the divalent to the trivalent state.

Essentially the content of this section has been the description of several examples of application of the method of K-line shifts to study the electronic mechanism of phase transitions in crystals. Sometimes the method offers only certain "conveniences." For example, the transitions in Fig. 10 can evidently be observed simply from the changes in the lattice parameters.[33]

---

[10] The assumption[19] of the effect of Eu via compression of the lattice owing to the lanthanide contraction seems dubious, since the difference is radii of Sm^{2+} and Eu^{2+} is quite insignificant (substantially smaller than their difference for the divalent and trivalent atoms, which explains the compression in the cases of Fig. 10a, b).

[11] As we know,[11] a semiconductor-metal transition occurs in SmSe at hydrostatic pressures of 40–50 kbar. Apparently it indicates an electronic phase transition in Sm. Thus perhaps the effective pressure developed by NdSe simply does not suffice.

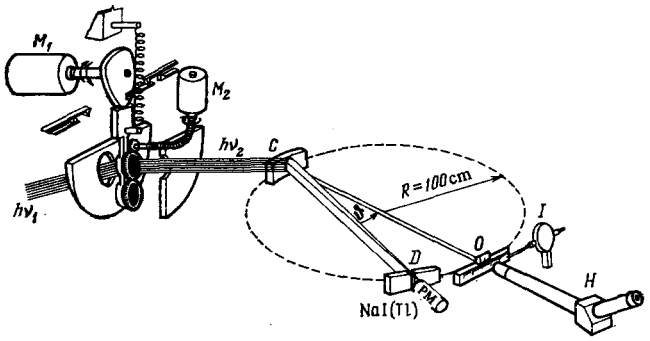

FIG. 11. Schematic diagram of a typical apparatus for measuring small shifts in K x-ray lines based on a Caucoois focusing diffraction spectrometer. Sources made of the compounds to be compared (dark circles in the diagram) are alternately introduced into the field of view of the instrument by the drive M1; M_2 is a motor that rotates the specimens, C is a single crystal bent into a cylinder with its axis at the point 0, with radius $\rho = 2R = 2$m; D is the entrance slit of the detector; and O, I, and H are the drive rod for rotating the crystal and measuring devices.

The merit of the method is its selectivity toward phenomena involving a change in the number of $4f$ electrons, since the very fact of the presence (or absence) of large K shifts unambiguously indicates the mechanism of the effects. At times it is very complicated to elucidate this by other methods (e.g., in the case of the Laves phases, Fig. 9). When necessary, these data can be confirmed by the curves of shift vs line type (facsimiles), which permit one to determine rather accurately also the fractions of $4f$ electrons participating in a transition. The latter arises from the relative simplicity of calibration of the effect, experimental and theoretical, which ultimately involves participation in the phenomenon of only the sufficiently deep-lying levels. To a rather good approximation, this allows one to treat the problem as a one-atom problem.

As we see it, a good application of this fundamental feature of the method is the example involving a self-consistent treatment of the problem under boundary conditions of the Wigner–Seitz type (see Fig. 5). This treatment allows one to establish a connection between the description of the phenomenon and the measured line shifts within the framework of a unified, rather rigorous calculation.

5. BRIEF INFORMATION ON THE PRINCIPLES AND DESIGN OF THE REQUIRED INSTRUMENTS

This chapter aims to give a brief description of the experimental methodology that should suffice to enable an interested reader to orient himself in the pertinent original publications.

At the same time, some problems pertaining to the principles of measuring small line shifts are presented in greater detail.

Figure 11 shows a diagram of a typical experimental apparatus.[36] The instrument is a Cauchois focusing diffraction spectrometer with a 2-meter focal length. The primary radiation $h\nu_1$ from an x-ray tube or an intense radioactive source[37] excites fluorescent x-rays $h\nu_2$ in one of the specimens (S_1, S_2) to be compared, which are introduced one after the other into the field of view of the instrument. Upon passing through a fixed diaphragm that limits the field of view to the central part of the working specimen, the beam $h\nu_2$ is incident of the monocrystalline plate C, which is bent into a cylinder of radius $\rho = 2R = 200$ cm. The plate is cut from a single crystal in such a way that crystallographic planes of interplanar spacing d coincide with the normal transverse cross-sections. The beam diffracted by the single crystal C while satisfying the Bragg condition $h\lambda = 2d\sin\vartheta$ is brought into a narrow line at the focus at the receiving slit of the luminescent detector D. The crystal can be rotated about the vertical axis near the Bragg angle by using a special mechanism, whereby the relative shifts are automatically measured (e.g., simply by counting the turns of the driving micrometer screw of the reducing mechanism) to an accuracy of the order of a second of angle.

Figure 12a explains the process of the measurements. They begin with one of the samples to be compared lying in the field of view of the instrument adjusted to a point (e.g., ϑ_1) on the shoulder of the line under study. Here the pulses from the detector are accumulated in the memory of the corresponding counting channel. After the necessary exposure (as a rule, 10–20 sec), the second of the specimens to be compared is introduced into the field of view of the instrument, and the pulses corresponding to it are accumulated in a second counting channel; here the diffraction angle is held constant at ϑ_1. This switch of specimens is repeated several times until the necessary "statistics" is accumulated, i.e., until the difference Δn_1 of the counts from the compared specimens is measured with the needed accuracy. Then the instrument is fixed at a new diffraction angle (ϑ_2 in Fig. 12a), and everything is repeated. Thus one systematically measures the entire twofold profile of the line (or, e.g., fourfold, depending on the number of specimens to be compared). If one knows the experimental differences Δn_i and the parameters of the profile (one assumes that the lines being compared are similar), one can easily calculate the sought line shift ΔE.

Evidently a question arises here that is very important for the success of this method that concerns the

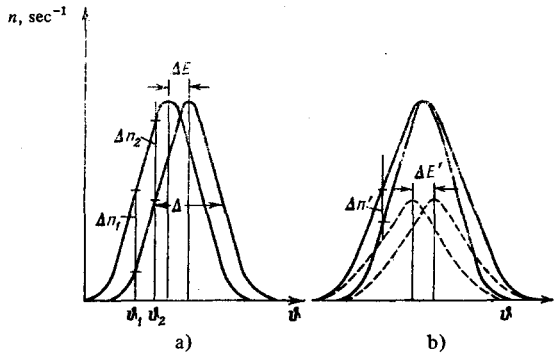

FIG. 12. Explanation of the process of the measurements and of the effect of possible deformations of the line profile.

conditions under which one can ensure the required similarity of the profiles of the lines being compared. Actually it is well known (in particular, see Ref. 38) that the intrinsic widths of the K x-ray lines amount to 0.2–0.3 mÅ, and they remain approximately constant (on the wavelength scale) over a broad range of Z values (e.g., from Mo to W). On the energy scale, this corresponds to intrinsic "physical" widths of the lines at half-height Δ_Φ in the range 5–50 eV. Thus the "anomalously large" shifts ΔE of the order of 1 eV corresponding to the $4f$ electrons amount in the rare-earth region to only about 1/30 of the natural line width. The ordinary experimental errors amount to from 10% to 1% of the effect, which corresponds to $\sigma(\Delta E)$ of the order 0.1–0.01 eV (see, e.g., Table I). This now corresponds to about 1/300–1/3000 of the line width. Evidently, the similarity of the lines under comparison must be assured to this degree of accuracy, i.e., physical or instrumental (aberration) effects that distort the shape of the compared lines should be absent.

A physical factor that distorts the profile is the appearance of fine structure in one of the lines being compared. For example, if the valence state of the second of the compared samples is an equilibrium mixture of two configurations $4f^n$ and $4f^{n-1}$, then the second of the compared lines will be an unresolved ($\Delta E' \approx 1$ eV, $\Delta_\Phi \approx 30$ eV) doublet with a distorted shape of the overall profile (Fig. 12b). However we can easily show that the following relationships hold for a rather wide class of spectral line shapes (in any case, for shapes of the Gaussian or Breit–Wigner types or mixtures of them):

$$\frac{\Delta n}{n} \sim \frac{\Delta E}{\Delta},$$

but

$$\frac{\Delta n'}{n} \sim \left(\frac{\Delta E'}{\Delta}\right)^2. \qquad (11)$$

Here Δn is the effect (see Fig. 12a) arising from a shift by the amount ΔE of a line of width Δ, and $\Delta n'$ is the effect (see Fig. 12b) of profile distortion caused by doublet character $\Delta E'$ of the lines.

When $\Delta E \approx \Delta E'$, we find that

$$\frac{\Delta n'}{\Delta n} \approx \frac{\Delta E}{\Delta} \ll 1, \qquad (12)$$

i.e., the distortion from the small effect proves to be of the second order of smallness, and cannot interfere with measuring the shift with an accuracy up to the same small magnitude. In other words, the very smallness (as compared with the line width) of the studied and the interfering effects ensures the needed rigidity and nondeformability of the line profiles.[12)]

[12)]This gives rise to the substantial difficulty of the inverse problem of seeking by an analogous method effects that lead only to line broadening. A good example is Ref. 39, which provided the first experimental demonstration of the effect of broadening of K_α lines arising from the so-called hyperfine splitting of the 1s level ($\Delta E' \approx 1$ eV) in the isotopes ^{151}Eu and ^{121}Sb. Here the obvious distinction was employed that the effect of a shift is an odd function with respect to the maximum, while the effect of broadening is an even function.

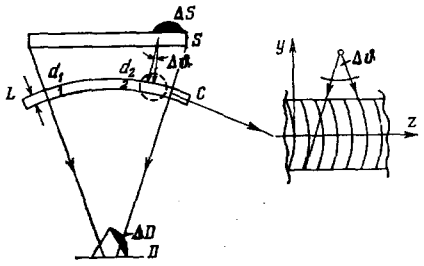

FIG. 13. Explanation of the role of the aperture aberration and of the effect of bending the reflecting planes on the acceptance angle $\Delta\varphi$.

The instrumental aberration effects present the main danger. Let us imagine that, owing to the imperfection of the single crystal C (Figs. 11, 13) or to an insufficiently precise preparation or bending of it, different regions of the crystal (1 and 2 in Fig. 13) focus the radiation into somewhat different regions of the focal circle (detector region in Figs. 11, 13), i.e., that the so-called aperture aberration is present. Now let us assume that one of the otherwise identical specimens under comparison has a brightness inhomogeneity somewhere in its area (ΔS in Fig. 13). To some extent, the latter is unavoidable even with the most painstaking preparation and standardization of specimens. Evidently, in the presence of aperture aberration, such an inhomogeneity will distort the line shape (ΔD in Fig. 13)—this is a parasitic shift in one of the profiles being compared. Some of the ways of combatting this phenomenon are trivial. The curve relating the line intensity to the specimen thickness in operating "in transmission" (the beams $h\nu_1$ and $h\nu_2$ pass through different surfaces of the specimen; Fig. 11) will evidently be a curve having a maximum. Specimen thicknesses that correspond to these maxima should be selected, since then not only will maximum line intensities be attained, but also the variations in brightness caused by inhomogeneities of the density or thickness of the specimens will be minimal. Moreover, one should rotate the specimens about an axis perpendicular to their surface (in the design of Fig. 11, this is carried out by the motor M_2). Here the possible brightness inhomogeneities will be smeared out into rings and, what is of particular importance, they will be symmetrized. One can naturally also try to diminish the aperture aberration itself that gives rise, as we have seen, to the aforementioned distortions. Therefore we require an accuracy of preparation and bending of the crystals that should approach "optical" accuracy, with the typical tolerances on plane-parallelism, planarity of the original monocrystalline plate, and deviations of its surface from an ideal cylinder after bending within the limits of one micron.

Yet, as we know, the very structure of actual crystals is not ideal. The deviations from ideal conditions consist of random rotations of individual small regions (mosaic blocks) of the crystal, which are characterized by the width of the angular distribution (usually close to Gaussian) of the mosaic blocks, and by a lack of constancy of the lattice parameters of the crystal, which is manifested in a certain variability of the interplanar spacing d of the system of planes employed for diffrac-

tion (see Fig. 13) for different regions of the area of the plate. Evidently this is one of the causes of aperture aberration.

Estimates show that from this standpoint the degree of perfection of real crystals that maximally approach ideal ones suffices, when they are characterized specifically by widths of the angular distribution of the mosaic blocks $\omega_\Gamma \lesssim 1''$ and $\Delta d/d \approx 10^{-5}$, as in the case of "semiconductor-grade" germanium and silicon, and also natural calcite, topaz, and quartz. But the radiation-gathering power turns out to be insufficient in x-ray spectrometers that use these crystals that are perhaps as close as possible to ideal ones. In somewhat simplified terms (a detailed presentation can be found in Ref. 40), the reason is that the mosaic spread determines the acceptance angle $\Delta\vartheta \approx \omega_\Gamma$ (see Fig. 13) of the instrument for the monochromatic radiation emitted by the atoms of the source. Hence, other conditions being equal, it is advantageous to have this acceptance angle as large as possible. On the other hand, $\Delta\vartheta$ can make its own contribution to the experimental line width. For example, when the studied components have a Gaussian shape, the latter is determined by the relationship

$$\Delta\vartheta_\Sigma \approx \sqrt{\Delta\vartheta^2 + \Delta\vartheta_\Phi^2}. \tag{13}$$

The optimum that corresponds to the maximal radiation-gathering power of the instrument in the case of a line that is yet practically unbroadened is then attained near

$$\Delta\vartheta \leqslant \Delta\vartheta_\Phi, \tag{14}$$

where $\Delta\vartheta_\Phi = \Delta\lambda/2d\cos\vartheta$ is the intrinsic (physical) line width, which is determined by differentiating the Bragg condition, and is estimated for $\Delta\lambda = 0.2$ mÅ (cf. above) with the typical $d \approx 1$ Å and $\cos\vartheta \approx 1$ to be $\Delta\vartheta_\Phi \approx 20''$.

Thus the mosaic spread of crystals closest to ideal ones proves to be roughly twenty times ($\Delta\vartheta_\Phi/\omega_\Gamma \approx 20''/1'' = 20$) smaller than the optimum. Correspondingly a diffraction spectrometer that employs a single crystal close to an ideal one will have a radiation-gathering power twenty times smaller than the optimum.[13] One might try to "spoil" a single crystal artificially by increasing the mosaic spread in a way similar to what is done, e.g., in neutron-diffraction spectroscopy when single crystals of so-called prolytic graphite are used. However, the growth of single crystals with a preassigned mosaic spread constitutes a very complicated technological problem. Moreover, there is always the danger in increasing the mosaic spread of also increasing the overall imperfection of the crystal, and in particular, the variations of the interplanar spacing Δd that determine the aperture aberration discussed above.

A way out has been found in employing the effect of elastic quasimosaicity,[40,41] which is inherent in ideal single crystals, and which simulates the needed, precalculated mosaicity while preserving the extreme homogeneity and perfection of the rest of the parameters. As

[13] We assume that the well-known thick-crystal condition is satisfied.

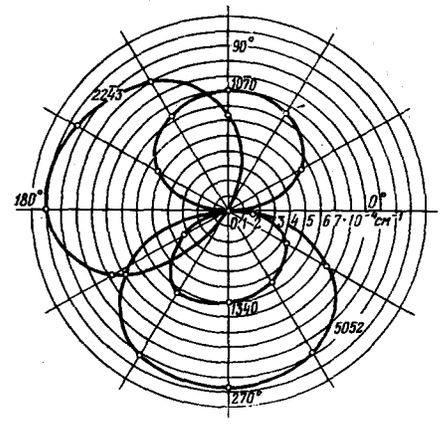

FIG. 14. Relationship of the bending coefficient k of the reflecting planes to the angle φ for a series of quartz plates bent into a cylinder of $\rho = 200$ cm. The curves are marked with the indices of the planes that coincide with the normal cross sections of the plates.

we know, when a plate made of an isotropic material is bent, the transverse cross sections normal to the longitudinal axis remain planar (Bernouilli's theorem). However, it is no less well known (see, e.g., Ref. 42), that this theorem is not valid in the general case of bending a plate made of an anisotropic material. It has been shown[41] that in a cylindrically bent plane-parallel plate of a focusing diffraction instrument, the reflecting planes coinciding with the normal transverse cross-sections are bent (see the inset in Fig. 13) along parabolic surfaces:

$$z = ky^2, \tag{15}$$

where

$$k \approx \left(a_{34} - \frac{a_{45}}{a_{55}}a_{35}\right)\left[2\rho\left(a_{33} - \frac{a_{35}^2}{a_{55}}\right)\right]^{-1}$$

is the bending coefficient, which depends on the components a_{ij} of the elastic tensor of the single crystal, which generally differs from zero. We easily note that the acceptance angle $\Delta\vartheta$ is now determined by the angle between the extreme tangents to the parabolas

$$\Delta\vartheta = 2kL, \tag{16}$$

where L is the thickness of the plate.

After one has selected the reflecting plane of the plate to be cut, and aligned the normal transverse cross-section with it, there still remains another degree of freedom: the possible rotations φ of the plate about the longitudinal z axis. Under such a rotation, the chosen crystallographic planes will remain coincident with the normal transverse cross-sections, and the parameters that characterize diffraction by the unbent crystal will also remain invariant. However, the bending coefficient k will vary as the components of the elastic tensor transform upon rotation. Figure 14 shows as an example the $k(\varphi)$ relationships calculated[40] for quartz plates in a series of orientations (the curves are marked with the indices of the planes that coincide with the normal

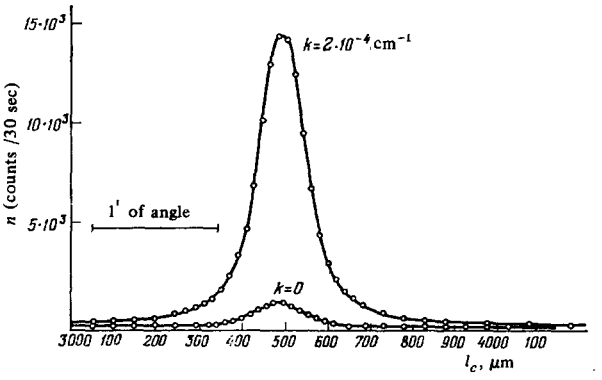

FIG. 15. The $K_{\alpha'}$ x-ray line of Sn. Obtained on a 2-meter Cauchois spectrometer (see Fig. 11) by using quartz plates with $13\bar{4}0$ planes coinciding with the normal cross sections for $k = 0$ and $k = 2 \times 10^{-4}$ cm^{-1}. The abscissa is the displacement of the meter rod for rotating the crystal (in μm).

cross-sections) when bent into a cylinder of 2 m radius. The numerical values of k lie in the range

$$0 \leqslant k \leqslant 10^{-3} \text{ cm}^{-1}.$$

For plates of millimeter thickness, this ensures an acceptance angle of

$$\omega_r \leqslant \Delta\vartheta \leqslant 2 \cdot 10^{-4} \text{ radians} = 40'', \qquad (17)$$

This excellently satisfies the optimal relationship (14), including even the most perfect crystals having the minimal mosaic spread ($\omega_r < 1''$).

Figure 15 shows the experimental K_{α_1} lines of Sn taken[40] with a 2 m focusing Cauchois spectrometer having millimeter single crystals of natural quartz ($\omega_r \lesssim 0.5''$) in which reflection from $13\bar{4}0$ planes coinciding with the normal transverse cross sections was employed. The lower curve was obtained from a plate having

$$k = 0 \quad (\Delta\vartheta \approx \omega_r \approx 0.5'').$$

The upper curve was obtained with

$$k = 2 \cdot 10^{-4} \text{ cm.}^{-1} \quad (\Delta\vartheta = 2kL = 4 \cdot 10^{-5} \text{ radians} = 8''),$$

all other conditions being kept identical. With practically identical line widths, employment of the elastic quasimosaicity effect increased the peak intensity of the line by a factor of 11.

Diffraction spectrometers optimized by the described method, and using commercially available x-ray apparatus for exciting fluorescence (e.g., RUP-200 or RUP-150) with currents of 10–20-mA, allow one to collect from 10,000 to 100,000 counts/min from specimens the size of a kopeck containing masses of the studied compounds of 100–300 mg. This allows one to obtain a standard result of the type shown in Table I, during a day of measurement on the average.

We should note in conclusion, that although practically all the currently existing data have been obtained with diffraction instruments similar to those that we have discussed. A possibility exists in principle of employing a quite different technique based on silicon or germanium semiconductor detectors. The first study of this type known to us is the measurement of the shifts of the $K_{\alpha_{1,2}}$ and $K_{\beta_{1,3}}$ lines for EuF_3–EuF_2 (see Table I, values marked with an asterisk), which was carried out with a standard Ge(Li) detector with a resolution of the order of 1 keV.[43] As we see, the attempt is quite successful, and shows that here also one can reduce the errors to 10^{-4} of the line width if the condition of identical geometries and intensities for the sources being compared is strictly satisfied. Employment of the best modern semiconductor detectors having a resolution of the order of 0.2–0.3 keV apparently allows one to attain an accuracy quite comparable with diffraction.

6. CONCLUSION

We have examined the effects of shifts of K_{α_1}, K_{β_1}, and $K_{\beta_{2,4}}$ lines of the order of one electron-volt involving a change in the number of $4f$ electrons in compounds of the rare-earth elements. They happened to be detected[14] and began to be studied later than smaller shifts of a different nature.

Now shifts that are weaker by factors of tens and hundreds are accessible to measurement. The most varied physical causes can be responsible for these shifts, including such effects as an alteration in the charge radii of isotopic nuclei, the above-mentioned hyperfine broadening of x-ray lines, and the study of correlation phenomena in atomic shells. The chemical applications (or, if one prefers, those pertaining to the physics of chemical bonds) become considerably broader at this level of magnitude of effects, e.g., those allowing (in quantitative combination with Mössbauer data) solution of such subtle problems as the determination of the valence structure of oxygen compounds of iodine with participation of s and p electrons and dative d bonds.[44] The interested reader can get an overview of this from the reviews.[31,45–48]

As for the future in the field closest to that which we have discussed here, the agenda includes the problem of analogous studies of the valency of the actinides. Attempts along this line have already been undertaken.[49,50] Yet, on the whole, the situation here is considerably more complicated, and this method has taken only the first steps.

[1]V. I. Spitsyn, Radiokhimiya **16**, 659 (1974).
[2]A. A. Chaikhorskiĭ, Radiokhimiya **17**, 263 (1975).
[3]W. H. Zachariasen, J. Inorg. and Nucl. Chem. **35**, 3487 (1973).
[4]P. W. Bridgman, Proc. Amer. Ac. Arts and Sci. **58**, 166 (1923).
[5]W. H. Zachariasen, Phys. Rev. **76**, 301 (1949).
[6]L. Pauling, J. Chem. Phys. **18**, 145 (1950).
[7]K. A. Geshneĭder, Splavy redkozemel'nykh metallov (Alloys of the Rare-Earth Metals), IL, M., 1965.
[8]R. Ramirez and L. M. Falicov, Phys. Rev. **B3**, 2425 (1971).
[9]V. A. Shaburov, I. M. Band, A. I. Grushko, T. B. Mezentseva, E. V. Petrovich, Yu. P. Smirnov, A. E. Sovestnov, O. I. Sumbaev, M. B. Trzhackovskaya, and I.V. Markova, Zh.

Eksp. Teor. Fiz. **65**, 1157 (1973) [Sov. Phys. JETP **38**, 573 (1974)].
[10]S. M. Blokhin, É. E. Vaĭnshteĭn, and V. N. Bertenev, Fiz. Tverd. Tela (Leningrad) **7**, 3558 (1965) [Sov. Phys. Solid State **7**, 2870 (1966)].
[11]A. Jayaraman, V. Narayanamurti, E. Bucher, and R. G. Maines, Phys. Rev. Lett. **25**, 1430 (1970).
[12]M. B. Maple and D. Wohlleben, *ibid.* **27**, 511 (1971).
[13]V. A. Shaburov, A. I. Egorov, G. A. Krutov, A. S. Ryl'nikov, A. E. Sovestnov, and O. I. Sumbaev, Zh. Eksp. Teor. Fiz. **68**, 326 (1975) [Sov. Phys. JETP **41**, 158 (1975)].
[14]O. I. Sumbaev, Yu. P. Smirnov, E. V. Petrovich, V. S. Zy Zykov, and A. I. Grushko, Pis'ma Zh. Eksp. Teor. Fiz. **10**, 209 (1969) [JETP Lett. **10**, 131 (1969)].
[15]Yu. P. Smirnov, O. I. Sumbaev, E. V. Petrovich, V. S. Zykov, A. I. Egorov, and A. I. Grushko, Zh. Eksp. Teor. Fiz. **57**, 1139 (1969) [Sov. Phys. JETP **30**, 622 (1970)].
[16]P. L. Lee, E. S. Seltzer, and F. Boehm, Phys. Lett. **A38**, 29 (1972).
[17]A. I. Grushko, A. I. Egorov, G. A. Krutov, T. B. Mezentseva, E. V. Petrovich, Yu. P. Smirnov, and O. I. Sumbaev, Radiokhimiya **20**, 128 (1978).
[18]V. A. Shaburov, A. E. Sovestinov, and O. I. Sumbaev, Phys. Lett. **A49**, 83 (1974).
[19]A. I. Egorov, E. V. Petrovich, Yu. P. Smirnov, A. E. Sovestnov, O. I. Sumbaev, and V. A. Shaburov, Izv. AN SSSR Ser. Fiz. **40**, 395 (1976).
[20]I. M. Band and M. B. Trzhaskovskaya, Tablitsy sobstvennykh znacheniĭ énergii élektronov, plotnosteĭ vblizi nulya i srednykh znacheniĭ v samosoglasovannykh polyakh atomov i ionov (Tables of the Eigenvalues of the Electron Energy, Densities Near the Origin, and Mean Values in the Self-Consistent Fields of Atoms and Ions). Preprint of the Leningrad Institute of Nuclear Physics of the Academy of Sciences of the USSR No. 91, Leningrad, 1974.
[21]P. W. Anderson, Phys. Rev. **124**, 31 (1961).
[22]D. I. Khomskii and A. N. Kocharjan, Sol. State Comm. **18**, 985 (1976).
[23]J. T. Waber, D. Liberman, and D. T. Cromer, in: Proc. of the Conference on Rare-Earth Researches (Phoenix, Arizona), Ed. by Eyring, N. Y., 1965.
[24]E. V. Petrovich, Yu. P. Smirnov, V. S. Zykov, A. I. Grushko, O. I. Sumbaev, I. M. Band, and M. B. Trzhaskovskaya, Zh. Eksp. Teor. Fiz. **61**, 1756 (1971) [Sov. Phys. JETP **34**, 935 (1972)].
[25]B. Johansson, Phil. Mag. **30**, 469 (1974).
[26]D. R. Gustafson and A. R. Mackintosh, J. Phys. Chem. Sol. **25**, 389 (1964).
[27]D. R. Gustafson, J. D. McNutt, and L. O. Roelling, Phys. Rev. **183**, 435 (1969).
[28]R. F. Gempel, D. R. Gustafson, and J. D. Willenberg, *ibid.* **B5**, 2082 (1972).
[29]E. King, J. A. Lee, I. R. Harris, and T. F. Smith, *ibid.* **B1**, 1380 (1970).
[30]V. A. Alekseev, B. Ya. Zel'dovich, and I. I. Sobel'man, Usp. Fiz. Nauk **118**, 385 (1976) [Sov. Phys. Usp. **19**, 207 (1976)].
[31]F. Boehm, Isotope Shifts, Chemical Shifts and Hyperfine Interaction of Atomic *K* X-Rays in Atomic Inner-Shell Processes, N. Y., Academic Press, 1975, p. 412.
[32]M. E. Teslyuk, Metallicheskie soedineniya so strukturoĭ faz Lavesa (Metallic Compounds with the Structure of the Laves Phases), "Nauka," M., 1969.
[33]A. Jayaraman, E. Bucher, P. D. Dernier, and L. D. Longinotti, Phys. Rev. Lett. **31**, 700 (1973).
[34]J. F. Miller, L. K. Matson, F. J. Reid, and R. C. Himes, J. Phys. and Chem. Sol. **25**, 969 (1964).
[35]M. Avignon and J. Dumas, Sol. State Comm. **11**, 1115 (1972).
[36]O. I. Sumbaev and A. F. Mezentsev, Zh. Eksp. Teor. Fiz. **49**, 459 (1965) [Sov. Phys. JETP **22**, 323 (1966)].
[37]O. I. Sumbaev, A. F. Mezentsev, V. I. Marushenko, A. S. Ryl'nikov, and G. A. Ivanov, Yad. Fiz. **9**, 906 (1969) [Sov. J. Nucl. Phys. **9**, 529 (1969)].
[38]M. A. Blokhin, Fizika rentgenovskikh lucheĭ (Physics of X-Rays), Gostekhizdat, M., 1957.
[39]A. S. Ryl'nikov, A. I. Egorov, G. A. Ivanov, V. I. Marushenko, A. F. Mezentsev, A. I. Smirnov, O. I. Sumbaev, and V. V. Fedorov, Zh. Eksp. Teor. Fiz. **63**, 53 (1972) [Sov. Phys. JETP **36**, 27 (1973)].
[40]O. I. Sumbaev, *ibid.* **54**, 1352 (1968) [Sov. Phys. JETP **27**, 724 (1968)].
[41]O. I. Sumbaev, *ibid.* **32**, 1276 (1957) [Sov. Phys. JETP **5**, 1042 (1957)].
[42]S. G. Lekhnitskiĭ, Teoriya uprogosti anizotropnogo tela (Theory of Elasticity of an Anisotropic Body), Gostekhizdat, M., 1950 (Engl. Trans., Theory of Elasticity of an Anisotropic Elastic Body, Holden-Day, San Francisco, 1963).
[43]V. I. Marushenko, L. A. Poneno, and A. I. Smirnov, Preprint of the Physicotechnical Institute of the Academy of Sciences of the USSR No. 287, Leningrad, 1972.
[44]L. I. Molkanov, Yu. S. Grushko, I. M. Band, G. A. Shadrina, and M. B. Trzhaskovskaya, Zh. Eksp. Teor. Fiz. **70**, 2218 (1976) [Sov. Phys. JETP **43**, 1158 (1976)].
[45]O. I. Sumbaev, in: Studies on the Changes of Nuclear Charge Radii Using the Effect of X-Ray Line Isotope Shift. Nuclear Structure, Vienne, IAEA, 1968, p. 527.
[46]O. I. Sumbaev, Zh. Eksp. Teor. Fiz. **57**, 1716 (1969) [Sov. Phys. JETP **30**, 927 (1970)].
[47]O. I. Sumbaev, Proc. of Intern. Conference on Inner Shell Ionization Phenomena and Future Applications, U.S., Oak Ridge, 1972, 1972, p. 346.
[48]O. I. Sumbaev, in: Modern Physics in Chemistry, V. 1, N. Y., Academic Press, 1977, p. 33.
[49]V. M. Vdovenko, L. L. Makarov, *et al.*, Radiokhimiya **14**, 384 (1972).
[50]A. V. Tyunis, V. M. Samsonov, and O. I. Sumbaev, Kristalldifraktsionnyĭ spektrometr dlya izmereniya khimicheskikh smeshcheniĭ rentgenovskikh liniĭ *L*-serii aktinidov (A Crystal-Diffraction Spectrometer for Measuring the Chemical Shifts of the *L*-Series X-Ray Lines of the Actinides). Preprint of the Leningrad Institute of Nuclear Physics of The Academy of Sciences of the USSR No. 151, Leningrad, 1975.

Translated by M. V. King